

Gleaming and dull surface textures from photonic-crystal-type nanostructures in the butterfly *Cyanophrys remus*

Krisztián Kertész,¹ Zsolt Bálint,² Zofia Vértesy,¹ Géza I. Márk,¹ Virginie Lousse,^{3,4} Jean Pol Vigneron,^{3,*} Marie Rassart,³ and László P. Biró^{1,†}

¹Research Institute for Technical Physics and Materials Science, P.O. Box 49, H-1525 Budapest, Hungary

²Hungarian Natural History Museum, H-1088 Budapest, Baross utca 13, Hungary

³Laboratoire de Physique du Solide, Facultés Universitaires Notre-Dame de la Paix, 61 rue de Bruxelles, B-5000 Namur Belgium

⁴Ginzton Laboratory, Stanford University, Stanford, California 94305, USA

(Received 27 March 2006; published 31 August 2006)

Photonic-crystal-type nanostructures occurring in the scales of the butterfly *Cyanophrys remus* were investigated by optical and electron microscopy (scanning and transmission electron microscopy), reflectance measurements (specular, integrated, and goniometric), by fast Fourier transform analysis of micrographs, by modeling, and by numerical simulation of the measured reflectance data. By evaluating the collected data in a cross-correlated way, we show that the metallic blue dorsal coloration originates from scales which individually are photonic single crystals of $50 \times 120 \mu\text{m}^2$, while the matt pea-green coloration of the ventral side arises from the cumulative effect of randomly arranged, bright photonic crystallites (blue, green, and yellow) with typical diameters in the 3–10- μm range. Both structures are based on a very moderate refractive index contrast between air and chitin. Using a bleached specimen in which the pigment has decayed with time, we investigated the role of pigment in photonic-crystal material in the process of color generation. The possible biologic utility of the metallic blue (single-crystal) and dull green (polycrystal) textures both achieved with photonic crystals are briefly discussed. Potential applications in the field of colorants, flat panel displays, smart textiles, and smart papers are surveyed.

DOI: [10.1103/PhysRevE.74.021922](https://doi.org/10.1103/PhysRevE.74.021922)

PACS number(s): 42.66.–p, 42.70.Qs, 42.81.Qb

I. INTRODUCTION

Photonic crystals are characterized by a refractive index which remains invariant under the spatial translations of a crystalline lattice [1,2]. In well-defined frequency ranges, called “stop bands,” these materials, also called photonic band-gap (PBG) materials, can prohibit electromagnetic-wave propagation along specific directions, even with the very moderate refractive index contrasts found with biological materials [3]. These optical structures can be engineered to produce a variety of optical filtering functions.

In the past 15 years a steadily growing attention has been given to photonic crystals. The efforts of the physics and materials science community were motivated mainly by the potential application of these materials in optical computing [4,5], the manufacturing of more efficient lasers [6,7], and other exciting new phenomena, like those arising from the application of disturbances such as shock waves [8]. The manufacturing of large-area photonic crystals operating in the visible spectrum is still a challenging and expensive task, given present-day laboratory techniques, but as a result of extremely refined biological evolution paths [3,9–13], periodic dielectric structures which operate in this wavelength range happen to be common in nature. Because they are ready made for us and because they show a very high complexity, biological photonic-crystal structures will be an essential tool for building a useful knowledge of inhomogeneous optical media. Even with regard to theoretical and

computing tools, these very demanding structures already enforced the improvement of existing numerical techniques. The expected feedback is that the study of these samples and the self-assembly techniques that may lead to them will inspire the production of new structures for applications in all ranges of the electromagnetic spectrum. In this respect, it is of considerable importance to uncover as completely as possible the physical mechanisms used by biological systems for generating visual textures or for the radiative energy management [3]. In these studies, the elucidation of various questions related to speciation [14,15] may also be important, but the main objective here is to put the findings to work for improving or simplifying technology. This is not uncommon in science: many pharmaceutical products are derived from molecules patiently developed by nature while optimizing global life mechanisms.

The wings of butterflies are covered by scales in a regular “tiles on a roof” pattern. In general, the butterfly scales have lengths in the range of 150–200 μm , while their width varies between 30 and 75 μm . Although composed of units in the size of a micron, the regular micropattern in certain butterflies, like some representatives of the nymphalid genus *Morpho* [10,12,16,17], when observed macroscopically, may give an impression of a “metallic surface.” These butterflies exhibiting shiny, metallic wings have structural colors.

The production of gleaming, metalliclike glossy surfaces is, by experience, associated with reflections leading to very narrow ranges of emergence angles. Hue selection by a surface is a separate issue: it is actually associated with the filtering of white light through pigmentary absorption or with the separation of frequencies among transmitted and reflected light fluxes, possibly on spatial inhomogeneities. The

*Electronic address: jean-pol.vigneron@fundp.ac.be

†Corresponding author. Electronic address: biro@mfa.kfki.hu



FIG. 1. (Color online) The butterfly *Cyanophrys acaste* is shown here in a resting position, when the hind wing overlaps the forewing. The ventral faces of the wings are displayed, with a cryptic dull green color. *Cyanophrys remus* displays identical resting position.

strong specular reflection from a planar metal surface or a planar multilayer stack is an example of a strictly specular process, while the diffraction beams produced by one- or two-dimensional periodic gratings are another, less restricted. Emergence angle selection is related to the photon momentum conservation which follows from total or partial translational invariance in the diffusing surface structure. Bright and gleaming structural colors have therefore often been associated with highly correlated structures, and many examples are found on butterfly wing scales [10–12,16]. Dull or matt colors, by contrast, seem to always involve some form of long-range disorder and, at first glance, should not be indicative of the presence of a highly correlated local geometry.

The studies of photonic-crystal-type structures in butterfly wing scales [10–12,16] most frequently revealed structural coloration only on the dorsal surface of the wings. In the present paper we investigate the southeastern Brazilian butterfly *Cyanophrys remus* (Hewitson, 1868) (a close relative of the butterfly represented in Fig. 1), which has different photonic-crystal-type structures on the ventral (matt green color) and dorsal (metallic blue) surfaces of its wings, Fig. 2.

The genus *Cyanophrys* (Clench, 1961) belongs to the Eumaeini tribe of family Lycaenidae. Generally, males are vivid blue dorsally, indicating a role in sexual signaling, while the female coloration is somewhat more discrete, having silvery or pale blue dorsal color with wide black wing margins. The genus is Panamerican in distribution and comprises 15 recognized species [18]. While the individual perches, basks, or rests on leaf surfaces, the pea-green ventral wing coloration with the darker tornal lobe presumably has a role in a complex survival strategy (cryptic pattern plus false-head) [19]. When resting, *Cyanophrys* imagines adopt a position as shown in Fig. 1. The region of the ventral forewing, delineated by the dashed line in Fig. 2(b), is covered by the hind wing. In this part of the wing surface, none of the scales give rise to the structural pea-green color. This may be regarded as strong evidence that the green coloration is useful only when the butterfly is resting with closed wings, indicating that the pea-green is in fact a functional cryptic color.

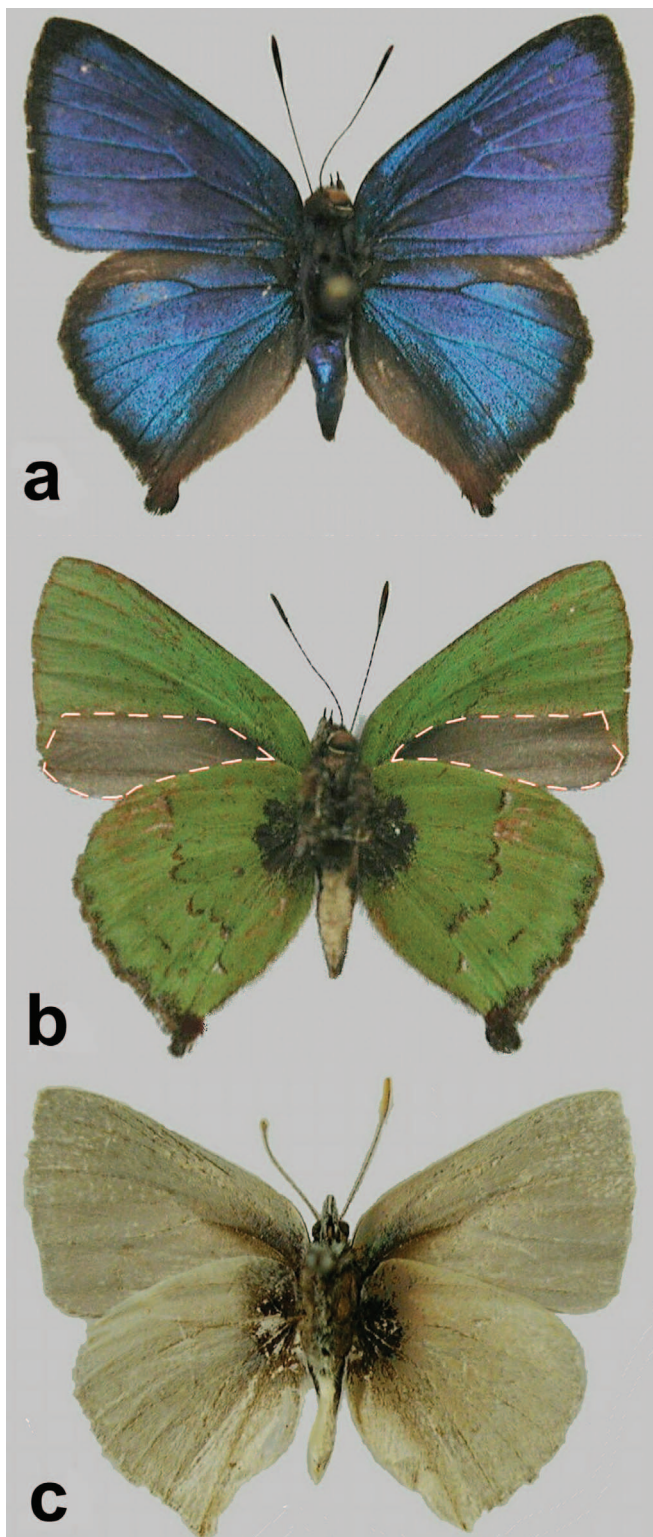


FIG. 2. (Color online) (a) Dorsal surface and (b) ventral surface of the butterfly *Cyanophrys remus* showing their structural colors. The region of the forewing delineated by dashed white lines is covered by the hindwings in resting position. It is worth pointing out that there are no scales producing structural colors along the ventral fore wing anal area. In (c) the ventral side of a bleached butterfly is shown (see text for details). All the specimens in this figure are males.

II. EXPERIMENTAL RESULTS

We investigated the scales on the wings of a male specimen of *Cyanophrys remus* originating from the Lepidoptera collection of the Natural History Museum, Budapest, Hungary, with label data “Brazil, Santa Catarina, São Bento do Sul, 600 m” (inventoried as No. 39 for the project). We studied the wings first by optical microscopy, then scanning electron microscopy (SEM), and transmission electron microscopy (TEM). Reflectivity measurements were carried out with an Avaspec 2048/2 fiber-optic spectrometer, both in specular arrangement under normal incidence and using a 3-cm integrating sphere in order to collect all the light reflected under any angle of emergence. All optical measurements were carried out with unpolarized light. An Avaspec diffuse, white standard was used as comparison sample for reflection factors measurements. A goniometric setup was used to measure reflectivity in nonspecular geometry. Microreflectivity measurements with a resolution below $3\ \mu\text{m}$ were carried out using the same fiber optic spectrometer in combination with an optical microscope. This allowed us to investigate details of color within one single scale. Both the dorsal wing (metallic blue) and the ventral wing (matt green) surfaces were investigated. To get more insight into the origin of color of this butterfly an old exemplar, exposed for several decades in a public exhibition [Fig. 2(c)], with the ventral side oriented to light, was also investigated. This aged butterfly completely lost its ventral pea-green color: it is bleached to a spectrally uniform reflectivity similar to that of a standard white reference in the whole spectral range from 450 to 800 nm.

A. Optical microscopy

Both wing pieces of several mm^2 and individual scales were studied. Once removed from the wing membranes using a sharp needle, individual scales were placed on a microscope slide and examined in transmitted and reflected light (the microscope aperture was 0.85, while the magnification was $60\times$). Surprisingly, optical microscopy reveals (in reflection) that the overall matt, pea-green coloration of the ventral wings arises from the mixing of very tiny, bright, blue, green, and yellow spots randomly distributed over the scale (see Fig. 3). The dominant color and the intensity of the bright localized reflectors show a significant sensitivity to the observation and illumination directions, indicative of a local structural coloration. In transmitted light, the ventral scales very clearly exhibited the expected granular structure. As Fig. 4(a) shows, the presence of brown melanin was identified only in the grains (the crystallites identified in the ventral scales) and the rest of the scale appears to be exempt of any pigment. We separately removed single cover and ground scales, and we examined them in the optical microscope under transmission and reflection conditions. This made clear that only the cover scales contained pigments. Most of the scales of the old, bleached butterfly were found deformed, as in the early stage of scroll formation, curving along the transversal (short side) direction. The extremely fragile ventral scales of the bleached butterfly showed only very weak pigmentation traces. The presence of grains was

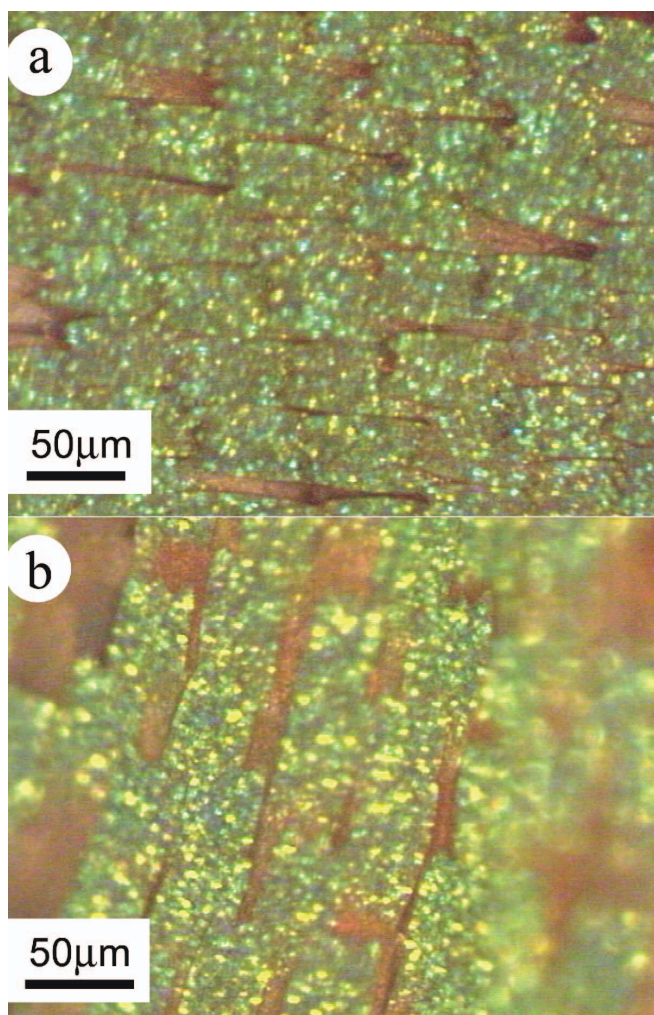


FIG. 3. (Color online) Ventral surface of the wing under two different conditions of illumination. One may remark the occurrence of bright spots colored blue, green, and yellow, which light up with different intensities as the illumination and observation conditions change.

also observed in this bleached specimen, as testified by Fig. 4(c), but in reflected light, as compared to the green scales [Fig. 4(b)], the bleached scales could only show a pale blue coloration in some of the grains [Fig. 4(d)]. Recent studies indicate that melanin may undergo irreversible alterations under UV illumination [20], so the loss of color in the bleached butterfly can be explained by the lack of melanin in the grains due to long exposure to the daylight.

B. Scanning electron microscopy and transmission electron microscopy

SEM samples were prepared by cutting pieces of the wing and by attaching them to double-sided conductive tape, followed by the deposition of 15 nm of sputtered gold, to allow examination in the SEM without charge buildup. Cross-sectional TEM samples were prepared by first incorporating pieces of wings in a plastic bloc, out of which sections of 70 nm thickness were cut by an ultramicrotome and trans-

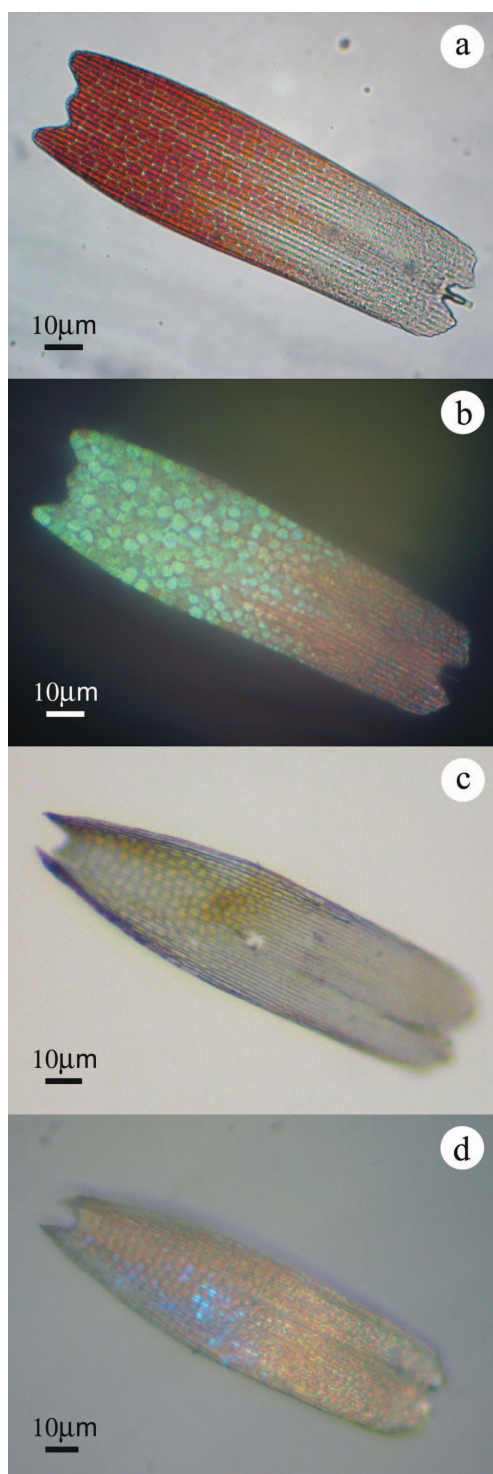


FIG. 4. (Color online) Optical microscopy images of the green scales on the ventral side of the wing: (a) and (b) of the normal specimen and (c) and (d) of the bleached specimen. (a) Light is transmitted through the scale (note the grain structure and the presence of brown pigment only in the grains); (b) light is reflected from the scale, and the grains light up with strong colors; (c) light is transmitted through the scale, the granular structure is still visible, and some very weak traces of pigmentation can be observed; (d) light is reflected from the scale, and only very weak traces of bluish color are visible on some grains. Note that the scale of the bleached butterfly is half scrolled.

ferred to copper grids. Inherently, this procedure does not allow the precise orientation of the sections with respect to the main geometric features of the scales.

1. Dorsal scales

The scanning electron microscopy investigation of bright metallic blue dorsal-wing scales showed that the entire scale of $50\ \mu\text{m}$ in width and $120\ \mu\text{m}$ in length is covered by a so-called “pepper-pot structure” [21], responsible for the color generation. The denomination pepper-pot structure is used by entomologists to designate a structure resembling that of inverted opal, with variable degrees of disorder. Here, opposite to the general case [21], the observed pepper-pot structure exhibits an unusual long-range order in the form of a regular crystalline pattern. Tilley and Eliot [21] investigated the scales of 48 lycaenid butterflies and we have ourselves investigated 58 Lycaenidae species and a dozen of species representing the lepidopteran families Nymphalidae, Papilionidae, and Zygaenidae. None of these earlier studies has ever exhibited such a perfect long-range order in the pepper-pot structure, extending all over the scale. The discovery of this long-range order in the scanning electron microscope images was, in the present case, hindered by the nearly continuous layer made by the ridges and cross ribs which cover a large part of this pepper-pot structure [Fig. 5(a)].

The combined use of SEM and TEM is often beneficial. In Fig. 5(b), a cross-sectional TEM image across the body of a scale close to the plane perpendicular onto the plane of the regular pepper-pot structure [Fig. 5(a)] is shown. It is apparent that the pepper-pot structure, visible through the “windows,” completely fills the entire volume of the ridges. The structure, if examined in detail, seems to exhibit a relatively high degree of long-range order. The observation of this order is, to some extent, hindered by the following facts: (i) none of the microscopic techniques in use (SEM and TEM) allows us to obtain a complete set of three-dimensional information pieces. (ii) While in the SEM the sample can be freely tilted, in TEM, it is not easily feasible to orient the plane of the sectioning during the sample preparation. (iii) The windows [Figs. 5(a) and 5(b)] are placed at relatively large distances from each other, compared with the size of the holes in the pepper pot structure. These holes seem to distribute on the nodes of a triangular lattice, which can be associated with the (111) plane of a face-centered-cubic (fcc) lattice or with an hexagonal primitive lattice. (iv) The structure seen in the cross-sectional TEM image shows a certain curvature in the plane of the section [Fig. 5(b)]. Therefore a careful correlated examination of the SEM and TEM images has to be carried out, and obtaining a full three-dimensional description of these chitin structures is far from being straightforward. Electron tomography was used by Argyros *et al.* to reveal the details of a somewhat similar structure [22] and, as they point out, (i) the appearance of the structure is strongly dependent on the position and the orientation of the sectioning plane and (ii) a number of 20 sections of $30\ \text{nm}$ thickness with minimum distortion would be needed to completely solve such a structure. This would demand a significant improvement of the actual sectioning techniques

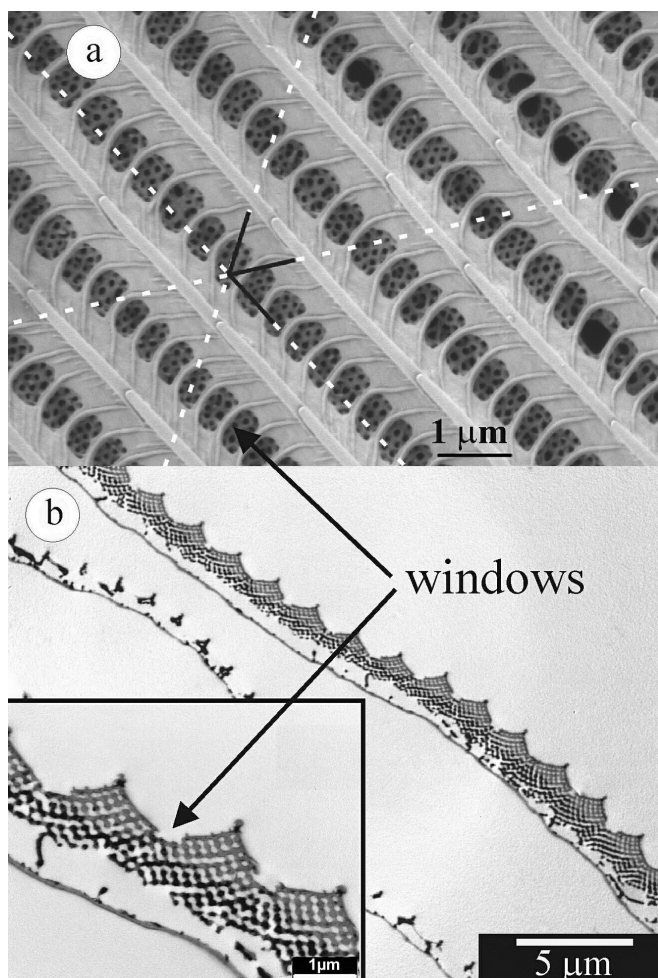


FIG. 5. Electron microscopic images of the wing scales of the normal specimen's dorsal surface. (a) Scanning electron microscopy image; the dotted white lines indicate the axes corresponding to the triangular lattice. The white lines have been placed manually as a best fit to the arrangement of holes, while the short, solid black lines were generated by 60° and 120° rotations, respectively, of a first line placed arbitrarily over one of the broken white lines. (b) Cross-sectional transmission electron microscopy images through the dorsal scales; the inset shows a magnified region of the photonic-crystal structure in which the details of the ordered structure are visible.

and is not within the reach or in the purpose of the present paper.

In order to get insight into the structure, detailed SEM and TEM images were cross correlated with computer modeling and two-dimensional Fourier analysis. In the SEM image depicted in Fig. 5(a), the white dashed lines help guide the eye through a coherent array of holes arranged, showing that they occupy the nodes of a triangular lattice, even when considered under *very distant* windows. The lines were arranged manually in a best-fit manner. Then, a short black line was laid over one of the white dashes lines, and the line was rotated by software over 60° and 120° , respectively. One can observe that the black lines fit perfectly with the dashes white ones, identifying the threefold symmetry expected on a triangular lattice. In a second step, the Fourier power spectrum of the image was calculated (Fig. 6).

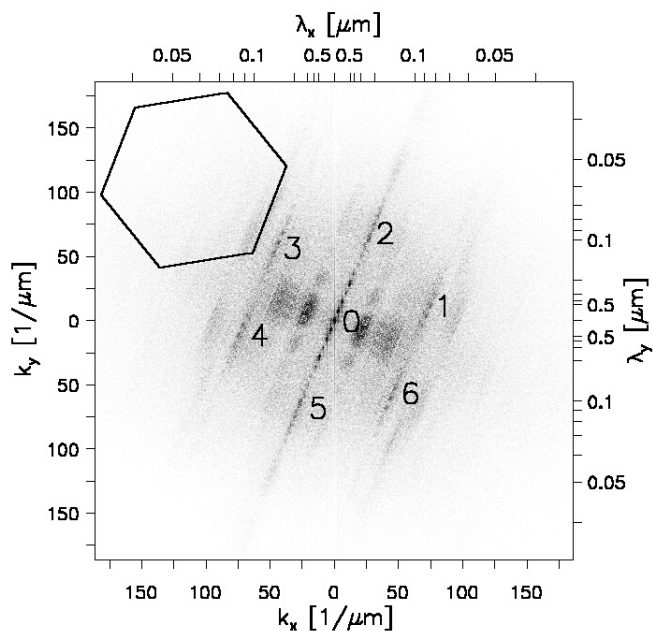


FIG. 6. Two-dimensional Fourier power spectrum of the SEM image of a scale from the dorsal side. White corresponds to zero intensity and black to maximum intensity. Wave number (wavelength) scale is shown on the lower and left (upper and right) axis, respectively. Numbers denote the peaks corresponding to the triangular lattice. These peaks form a hexagon, shown schematically in the upper left corner. See the text for details.

The interpretation of the resulting pattern is not a straightforward task as the image is constituted from three different kinds of periodically arranged objects, with hierarchic sizes: (i) the ridges, (ii) the windows, and (iii) the holes forming the triangular lattice. The typical dimensions of the various structural elements characteristic for the dorsal scales, as measured from SEM images, are given in Table I. In order to analyze the long-range periodic patterns present in the photonic crystal structure, we performed a detailed Fourier analysis of the SEM images. Besides analyzing the experimental SEM images, we also built model images (see Discussion), in order to understand better the results and in order to separate the contribution of the different components of the structure to the Fourier image. Figure 6 shows the gray scale image of the two-dimensional (2D) Fourier power spectrum of the SEM image of a dorsal scale. The image is unprocessed, apart from the application of a Hanning window function, in order to eliminate aliasing artifacts and of a nonlinear gray scale to enhance visualization of the peaks. At the center of the image there is a line of peaks with a periodicity of $\Delta k = 3.64 \mu\text{m}^{-1}$, forming an angle of 23° with the vertical direction. This corresponds, in real space, to a periodic array of lines separated by 1726 nm at 23° from the horizontal direction: the series of ridges. At a distance of $11.01 \mu\text{m}^{-1}$ from the central line of peaks we find two strongly blurred parallel lines of peaks at the left and right. The $11.01 \mu\text{m}^{-1}$ wave number corresponds to a wavelength of $\lambda = 566 \text{ nm}$, which is the just average separation of the windows in the direction along the ridges, as calculated from

TABLE I. Characteristic dimensions of relevant structural elements on the dorsal wing scales of butterfly *Cynophrys remus* as measured from electron microscopy images.

Structural feature	Dimensions (nm)	Standard deviation (nm)	Observation (Measured from)
Distance of the ridges	1502	± 111	SEM
Height of the ridges as measured from the level of triangular lattice visible through the “windows” [Fig. 4(a)]	617	± 80	TEM
Basal width of the ridges	937	± 69	SEM
Distance of the cross ribs	629	± 93	SEM
Width of the cross ribs	149	± 21	SEM
Window length (normal to the ridges)	665	± 30	SEM
Window width (parallel with ridges)	417	± 74	SEM
Hole diameter in the plane of the triangular lattice	103	± 12	SEM
Distance of hole centers in the plane of the triangular lattice	162	± 22	SEM

the values given in Table I (window width augmented by the width of the cross ribs). The blurring is caused by the non-uniform size of the rectangular windows [see the SEM image in Fig. 5(a)]. The two second-harmonic aligned spots are also visible, but the blurring is even more present. This central structure, composed of a central line of spots with two parallel, blurred, replica, is denoted by “0” in Fig. 6. This central structure is repeated symmetrically at six places (denoted by numbers “1”–“6”), forming the vertices of a hexagon of radius $35.9 \mu\text{m}^{-1}$, which corresponds to a wavelength of $\lambda = 175 \text{ nm}$, close to the average distance of the holes (see Table I). These six vertices can be identified with the triangular lattice of holes. The fact that the central line of spots is replicated at the vertices of the hexagon with practically no blurring is very important: it proves the presence of a long-range order and coherence in the triangular lattice of holes.

The cross-sectional TEM images shown in Fig. 5(b) make it possible two observations: (i) similarly like the long-range order outlined by the dashed white lines in Fig. 5(a), long-range order is also present in a transversal plane and (ii) the pepper-pot structure is not limited to the regions visible through the windows” of the mostly continuous top cover layer, but it constitutes the basic structure of the scale, filling the wide ridges, too. It is worth pointing out that the ridges, which are rigorously parallel to each other [Fig. 5(a)], contain, as a matter of fact, the most regular part of the pepper-pot filling from the body of the scale.

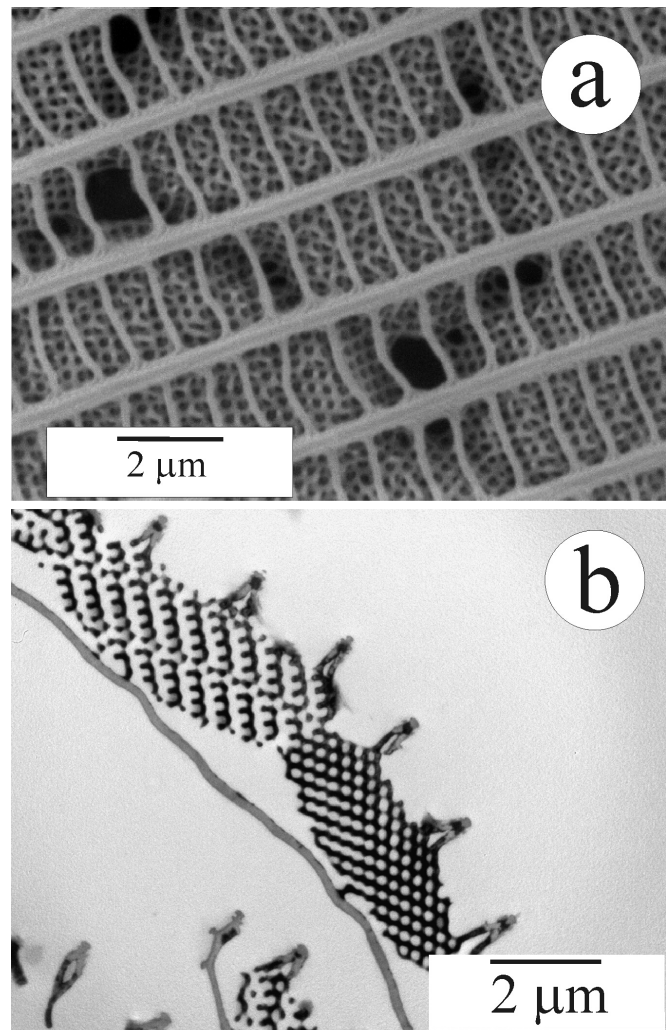


FIG. 7. Electron micrographs of the wing scales of the normal specimen’s ventral surface. (a) Scanning electron micrograph of the photonic crystal grains with random orientation in a green scale situated between the cuticular membrane of the individual scale and the network of the longitudinal ridges and cross ribs and (b) cross-sectional transmission electron micrograph through an individual green scale; one may notice the precise regular structure within one grain and the different orientation of the neighboring grains.

2. Ventral scales

The electron microscopic examination of the ventral side of the wings revealed scales with a rather peculiar structure: between the ventral cuticular membrane of the scale and the network of ridges and cross ribs, we find small grains with typical diameters in the $5\text{--}10\text{-}\mu\text{m}$ range. These grains show a regular structure, to some extent similar to the homogeneous pepper-pot filling of the dorsal scales. Opposite to the long-range order found in the dorsal scales, the orientation of these grains with respect to each other is random, Fig. 7. The grains seem to exhibit an internal fcc inverted opal structure. The regularity of the structure *within one single grain* is convincingly revealed by the cross-sectional TEM images in Fig. 7(b). These grains act as individual photonic crystallites and, depending on the orientation of the incident light and

TABLE II. Characteristic dimensions of relevant structural elements on the ventral wing scales of the butterfly *Cynophrys remus* as measured from electron microscopy images.

Structural feature	Dimensions (nm)	Standard deviation (nm)	Observation (Measured from)
Distance of the ridges	1957	± 54	SEM
Diameter of the holes	178	± 34	SEM
Distance of the center of holes	280	± 39	SEM
Distance of cross ribs	772	± 71	SEM

the observation angle, give rise to the bright colors spots detected in optical microscopy (Fig. 3). The summation of the colors and the random orientation of the grains may be responsible for the matt, pea-green coloration of the ventral scales. If the entire scale were covered by a single photonic-crystal grain, like on the dorsal scales, its metallic aspect would greatly hinder the cryptic effect. The characteristic dimensions of the fcc inverted opal structure are spherical voids of 178 ± 34 nm in diameter with centers at a distance of 280 ± 39 nm, respectively. Other relevant dimensions are given in Table II.

C. Spectroscopy

The reflectance spectra measured on complete wings under normal incidence, collected specularly and with the integration sphere, Fig. 8, show remarkable features. While on the dorsal side we find a slight difference in the frequency locations of the (specular or hemispherical) reflectance maxima, on the ventral side there is no such difference. Also, the bleached butterfly (no melanin in the grains) has a neutral color close to that of the diffuse reflectance standard, Figs. 8(a) and 8(b). The shift between the spectral positions of the reflectance maxima measured on the dorsal side under normal incidence and with the integration sphere indicates that the reflectivity may be angle dependent. A further feature worth being pointed out is that, contrasting the case of a usual diffuse reflector, the integrated measurement exhibits a peak higher than the specular one at normal incidence. In the case of the ventral green, the color is practically independent of the viewing or illumination angle (no shift between the integrated and specular measurement), which may be related to averaging of the effects of the large number of randomly oriented photonic crystal grains of different colors. Opposite to the case of the dorsal wing, the integrated reflectance peak—as usual—is smaller than the specular one obtained under normal incidence.

The normal (not bleached) butterfly changed the dorsal blue color to green and the ventral green to pale orange-red when wetting with ethanol was applied. Both surfaces completely recovering their original coloration after the evaporation of the alcohol. This indicates that due to the higher refractive index of ethanol as compared with air, the photonic band gap of the structures is redshifted when filled with

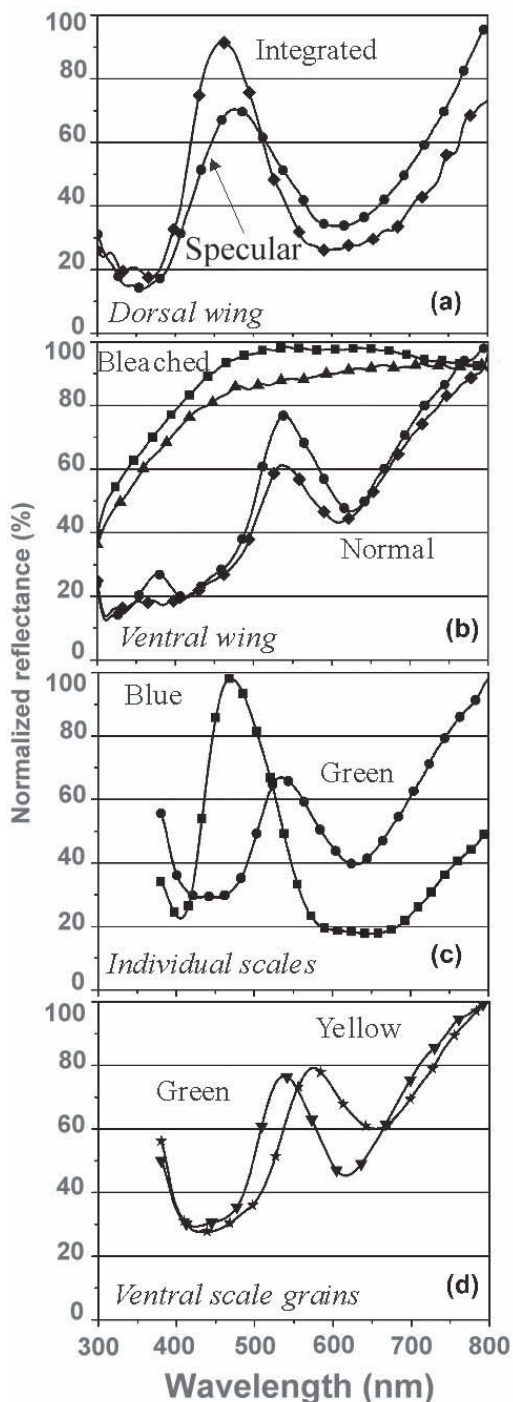


FIG. 8. Reflectance spectra of the butterfly wings, individual scales, and grains. To make possible comparisons all spectra have been normalized to 100%. Specular reflectance was measured at normal incidence with respect to the wing plane. (a) Dorsal wing: the reflectance is measured in a specular geometry (circles) or with an integration sphere (diamonds). (b) Reflectance of the bleached ventral wing (squares for specular, triangles for integrated) and the green ventral wing (circles for specular, diamonds for integrated). (c) Microreflectance of individual blue scale (dorsal side) compared to the reflectance of an individual green scale on the ventral side. (d) Reflectance of individual grains on a scale from the ventral side, yellow grain (stars), compared to that of a green grain (triangles).

alcohol, in a similar way as reported for *Morpho* butterflies [23].

The microreflectance measurements carried out on individual scales, Fig. 8(c), eliminate the effects arising from the disorder that may be present in the orientation of individual scales when measuring a whole wing. These measurements indeed show that the width of the blue reflectance maximum is unchanged, compared with the value measured on the piece of wing (cumulated reflectance of many scales), but its relative intensity has increased. This may be linked to the not precisely defined incidence conditions when just one single scale is measured in the spectral microscope under normal incidence. In the case of the green ventral surface scales measured in the spectral microscope, as compared to the measurement on the piece of wing, no significant differences are observed; this is attributed to the randomness in the orientation of the photonic-crystal grains in the scale itself.

The single-grain measurements carried out on the bright green and yellow grains of micron size yielded reflectance spectra shown in Fig. 8(d). Comparing the reflectance of the ventral scale to these curves gives a further experimental proof for the existence of blue grains, as seen in Fig. 3. Without a certain fraction of blue, even a 50%–50% coverage by green and yellow grains would redshift the position of the global ventral reflectance maximum as compared with reflectance curve in Fig. 8(c). Although the blue grains can be observed under lower magnification, in the high magnification needed for reflectance measurements on one single grain they are not visible. The likely reason for this is the change in the incidence angle of light as magnification is increased. Computation, as seen below, predicts the possibility of a blue grain, but at the same time, sees it at very narrow band.

In order to investigate the dependence of the reflectivity on the incidence and emergence conditions, goniometric measurements were carried out. The goniometric reflectance measurements were performed under the arbitrarily chosen 45° angle of incidence with respect to the wing plane. Two different setups were used: (i) specular and (ii) backscattered, Fig. 9. The wing was rotated 360° parallel to itself, around the axis marked by the dashed line in Fig. 9, in steps of 10° ; in each position a full reflectance spectrum was recorded. The spectra were plotted in 3D; the result is shown in Fig. 10. To distinguish between the two opposite orientations when the light is coming from the edge of the wing towards the body of the butterfly, or in the opposite direction, the schematic scale in Fig. 9 shows a rodlike feature on the right-hand side, which corresponds to the scale pedicel (pointing towards the body of the butterfly) which fixes the scale into socket in the wing membrane.

It is remarkable to note the differences both in spectral and angular positions of the reflectance maxima (dorsal) and in their amplitude (dorsal and ventral). These effects may be associated to a certain extent with the fact that as in the case of most butterflies, the scales may deviate from the plane of the wing membrane by an angle around 10° . Other effects will be analyzed in the Discussion section.

A most remarkable feature is the increase in backscattered arrangement of the amplitude from around 30% to around 80% of the dorsal reflectance maximum and its splitting into

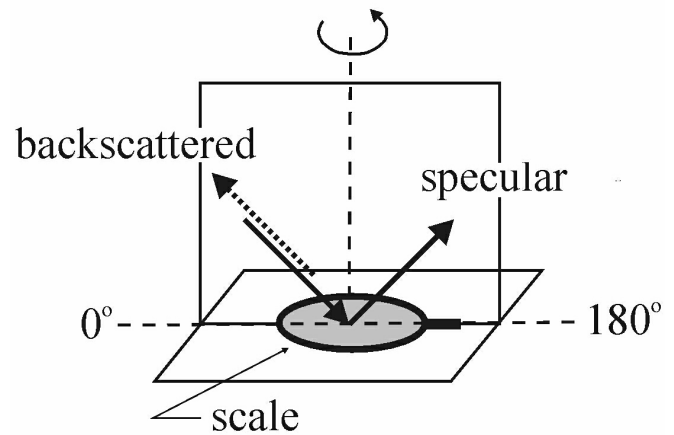


FIG. 9. Geometry for the goniometric reflectance measurements. The orientation of the scales is shown schematically by the shaded ellipse, with a “rod” on the right-hand side standing for the pedicel of the scale. The incidence angle was arbitrarily chosen to be 45° as measured from the plane of the wing. Two different setups were used: (i) specular and (ii) backscattered. The wing was rotated 360° parallel to itself, around the axis marked by the dashed line, in steps of 10° . In each position a full reflectance spectrum was recorded.

twin peaks, positioned at 120° and 240° , respectively. The two directions are placed at -60° and at $+60^\circ$ with respect to the orientation of the ridges. A similar increase in the amplitude from 18% to 60% is encountered in the case of the ventral reflectance maximum in the range of 550 nm. A more detailed discussion follows in Sec. III.

III. DISCUSSION

The correct interpretation of the SEM and TEM micrographs is not always straightforward. Furthermore, as pointed out by Argyros and co-workers [22] it is a rather complex task to obtain consistent 3D information from the synthesis of SEM and TEM data. Therefore we will start by discussing in more detail the structures revealed by electron microscopy.

As already mentioned in the experimental section, due to the complex structure of the dorsal scales, it is not easy to observe the long-range order present in the triangular lattice [Fig. 5(a)]. Fast Fourier transform (FFT) analysis is certainly a most helpful tool in the investigation of the structure. In order to be able to precisely identify the origin of the maxima observed in the Fourier power spectrum (Fig. 6), the simulation of the FFT power spectrum obtained from experimental data was carried out. The central structure (denoted by “0”) is replicated at the vertices of the hexagon (denoted by “1”–“6”) as a result of the convolution of the central structure with the six vertices. This phenomenon is analyzed in detail in Fig. 11. First we constructed the model of the SEM image based on measurements of the average characteristic length scales of the structure (Table I). The structure is composed of two substructures: the triangular array of circular holes [see Fig. 11(a)] and the rectangular array of rectangular windows [see Fig. 11(b)]. The triangular array of

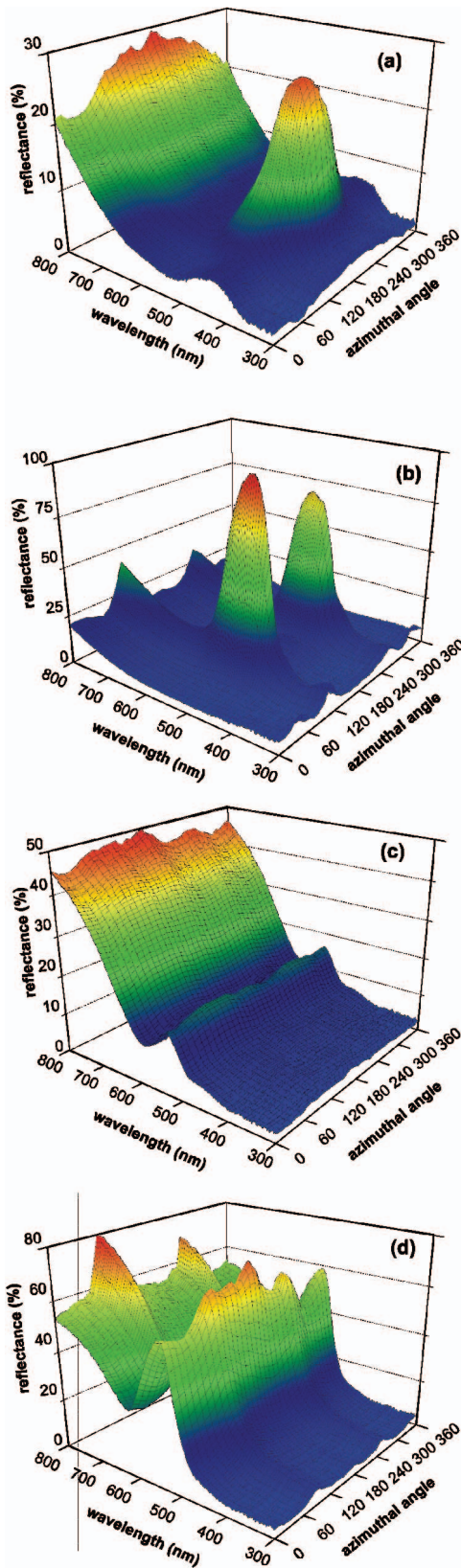


FIG. 10. (Color online) Spectrogoniometric measurements carried out according to the schematic arrangement shown in Fig. 9. For convenience, all data are normalized to 100%. Dorsal side: (a) specular and (b) backscattered. Ventral side: (c) specular and (d) backscattered.

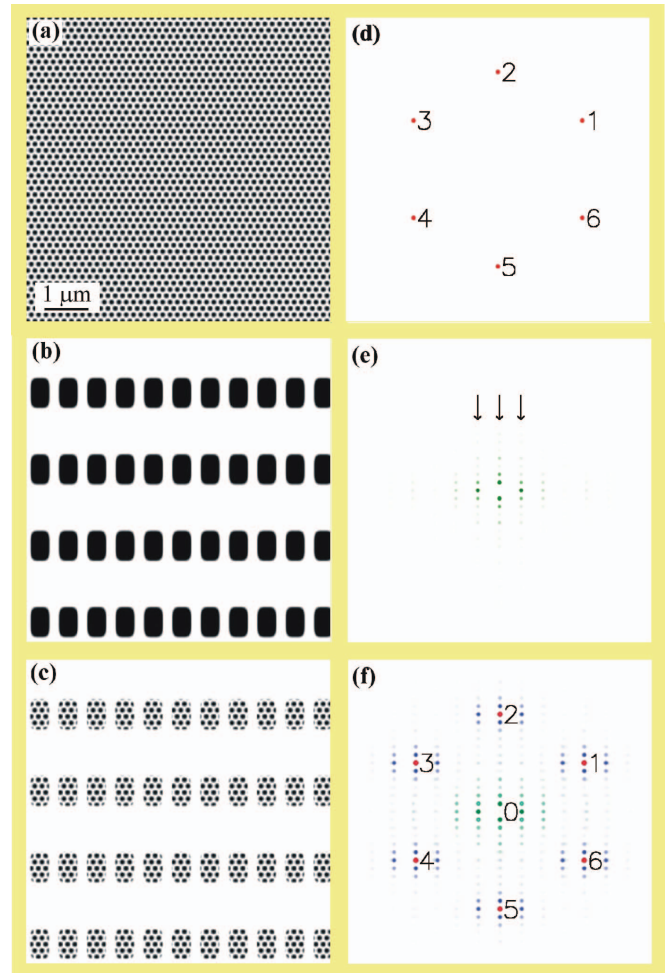


FIG. 11. (Color online) Simulated patterns (a)–(c) and their Fourier power spectra (d)–(f). (a) A triangular lattice of holes. (b) Rectangular lattice of rectangular windows with rounded corners. (c) The triangular lattice of holes seen through the windows. (d) and (e) Fourier power spectra of (a) and (b), color coded with red and green. (f) Composite color image of Fourier spectra of (a), (b), and (c) color coded with red, green, and blue. The numbers and arrows show the positions of the Fourier peaks. A small broadening was applied to the Fourier peaks in order to facilitate presentation. See the text for color coding and details.

holes was chosen to be a harmonic function, composed of three cosine waves at a 120° angle:

$$f(\vec{r}) = \sum_{j=1}^3 \cos(\vec{k}_j \cdot \vec{r}), \quad (1)$$

where

$$\vec{r} = (x, y) \quad (2)$$

and

$$\vec{k}_j = \frac{2\pi\sqrt{3}}{d_{\text{hole}}} \left(\cos 2j\frac{\pi}{3}, \sin 2j\frac{\pi}{3} \right). \quad (3)$$

The vertices of the rectangular windows were rounded and the edges of the rectangular windows were blurred in

order to model the measured SEM picture more accurately. The complete structure [Fig. 11(c)] is the array of holes masked by the array of windows. In a second step we calculated numerically the Fourier power spectrum of the two substructures [Figs. 11(d) and 11(e)] and that of the complete structure [Fig. 11(f)]. The numerical Fourier transform gave very thin peaks thanks to the perfectly periodic structures. In order to facilitate presentation a small broadening was applied to these peaks in Figs. 11(d)–11(f). As expected, the Fourier image of the perfect triangular lattice is composed of six peaks at the vertices of a hexagon (denoted by the numbers in the figure). There are no second- and higher-harmonic peaks because the lattice of holes is an harmonic function [see Eq. (1)]. Figure 11(e) is the Fourier image of the rectangular array of windows in Fig. 11(b). It is composed of parallel vertical lines of equidistant peaks in a rectangular arrangement. The four first-order peaks are the most prominent but some higher-harmonic peaks are also visible. The amplitude of the higher harmonics, however, is quickly decreasing. This is because the magnitude of the high-spatial-frequency components is negligible, thanks to the blurred edge of the rectangular windows. Figure 11(f) is the Fourier image of the complete model structure, Fig. 11(c). The Fourier transform of the complete structure is the convolution of the Fourier transforms of the two substructures: the rectangular array of peaks (denoted by “0” in the figure) corresponding to the windows is repeated at the positions of the vertices of the hexagon (denoted by “1”–“6” in the figure) corresponding to the holes.

The convolution process is further illustrated by color coding of Fig. 11(f), which is a composite red, green, and blue (RGB) color image of the three Fourier power spectra: the peaks corresponding to the holes (windows) substructure are coded in red (green) and the peaks corresponding to the complete structure are coded in blue. The red dots in the middle of the replicated structures at “1”–“6” mean that the central structure (corresponding to the windows) is repeated, centered at the vertices of the hexagon. The central structure itself is cyan in the composite image because the central structure also appears in the Fourier transform of the window array (denoted by green) and that of the complete structure.

The comparison of the experimental 2D FFT power spectrum (Fig. 6) with the one calculated from the simulated structure [Fig. 11(d)] convincingly confirms that indeed the lattice of holes seen in the SEM image shown in Fig. 5(a) is a triangular lattice exhibiting long-range translational symmetry. In other words, the complete scale may be regarded as a single crystal.

When comparing the distance of ridges in the SEM image with that of the TEM image in Fig. 5, one may conclude that there is a certain discrepancy. The difference originates from the fact that the plane in which the scale was sectioned is not perpendicular on the line defined by the direction of the ridges. The magnitude of the deviation of the TEM ridge distance brings information about the value of the angle between the direction of the ridges and of the sectioning plane; this value can be calculated using simple trigonometry as being 40° (Fig. 12). One can remark that despite the fact that the orientation of the sectioning plane is not falling rigorously onto one of the high-symmetry directions, the contrast

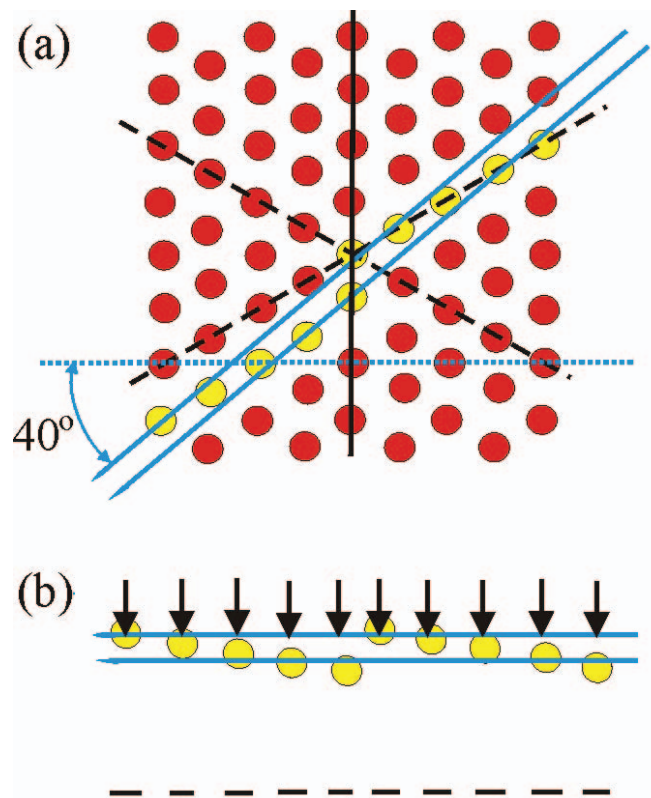


FIG. 12. (Color online) Orientation of the TEM section with respect to the main structural elements of the triangular lattice of holes (a) and TEM image formation of the section (b). In (a) a triangular lattice of holes is shown with the three characteristic axes outlined; the one drawn as a solid line is the one parallel with the ridges. The ideal orientation of the sectioning plane would be along the dotted line, while the real orientation is shown by the two parallel lines making an angle of 40° with the dotted line. The distance of the two parallel lines illustrates the fact that the section has a finite thickness. The holes which fall within the section are highlighted. In (b) the section is shown as illuminated by a homogenous electron beam. One may notice that the contrast arising from the different thicknesses of material through which the electrons travel (projecting the holes onto a plane) will exhibit a regular pattern.

pattern obtained in the TEM still appears to be a regular one, with relatively minor deviations from regularity, determined by the particular value of the misorientation. With this in mind it is worth examining in more detail the TEM cross sections.

In Fig. 13 a high-magnification TEM image [inset of Fig. 5(b)] is shown over which a pattern of lines was superimposed by joining the filled nodes of the structure according to the rule: first-neighbor nodes are joined by straight segments. To facilitate examination the network was shifted in the upper right corner of the image and corresponding nodes were joined by thin black lines. One may observe that the black lines are parallel and have the same length. This shows that the structure, although different from the usual single-crystal structures, has translational order in the plane of the section—i.e., in a plane perpendicular to the plane of the triangular lattice investigated in the SEM micrographs. Based on this observation, it is justified to make an attempt

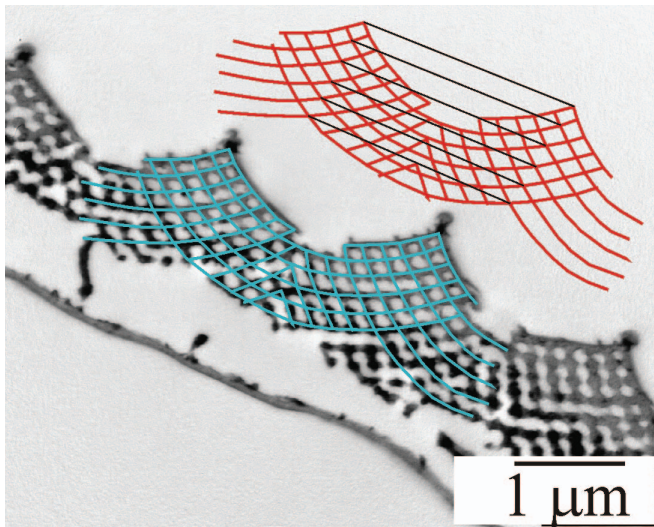


FIG. 13. (Color online) TEM image [inset of Fig. 5(b)] shown in detail with a network of lines superimposed on the TEM micrograph according to the following rule: neighboring filled nodes are joined by a straight line. The network obtained in this way is shifted to the right upper corner and thin black lines were used to join corresponding nodes. One may notice that the network has translational order in the plane of the section.

to reconstruct the full 3D structure by combining the SEM and TEM data.

The starting structure is a regular AAA stack of layers with a triangular pattern of holes. The AAA stacking corresponds to a primitive hexagonal lattice opposite to the ABAB stacking of a graphite type lattice, or the ABC stacking, which may yield a cubic structure. Such a stack is shown schematically in Fig. 14(a). After selecting a particular node in the topmost layer, a wedge shaped part of the stack is removed, followed by the folding of the two remaining halves into a “rodlike” object that has on both of its upper faces the triangular hole pattern [Fig. 14(b)]. In Fig. 14(c) using the obtained rods and a rectangular piece of the regular stack of layers from Fig. 14(a), a model structure is built corresponding to two ridges and an interridge region. In Fig. 14(c) in the two regions filled with lighter circles help connecting the elements from which the model structure is built. Stacking faults appear in the connecting regions, but the optical effect of these is negligible.

The model structure is fully consistent with the reflectance data. As shown schematically in Fig. 15, in the normal-incidence specular measurement, the light emerging along a normal direction is reflected on the structure seen through the windows; the light reflected from the sides of the ridges emerges under different angles. The maximum of this reflectance peak is situated at 480 nm; its relative amplitude is 70% [Fig. 8(a)]. When carrying out the integrated measurement, the peak position is shifted to 460 nm, indicating the presence of shorter-wavelength reflections. Furthermore, in a rather unusual way, the relative intensity of the maximum increases to 90%, showing that a significant fraction of the reflected light under specular incidence conditions was lost. This is fully consistent with the ratio of the area occupied by windows and that occupied by ridges [Fig. 5(a)].

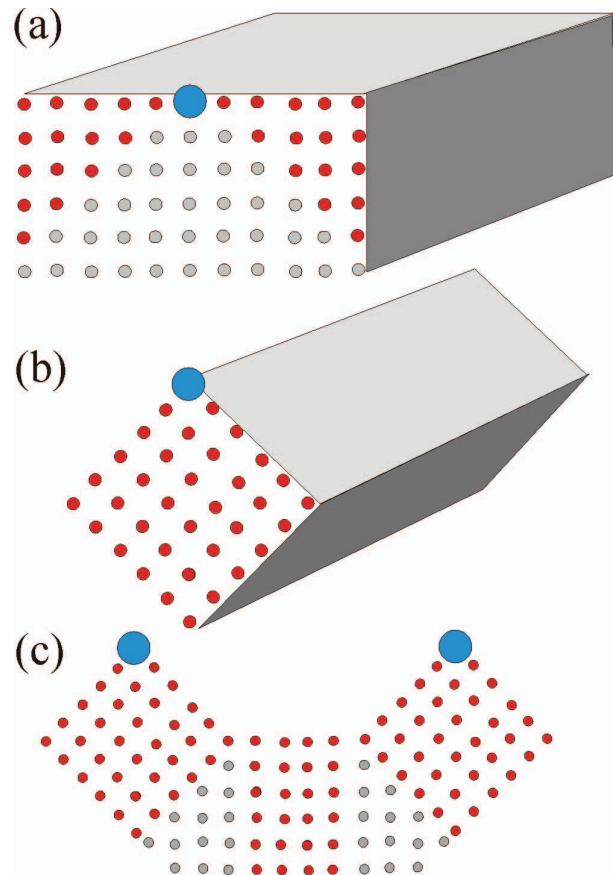


FIG. 14. (Color online) Schematic illustration of “folding” of ridges from a stack of layers with a regular triangular pattern of holes, only the holes facing the observer are shown. (a) In a regular stack of layers a node (larger circle) is selected and a wedge shape part (lighter circles) is removed; (b) after folding the two halves of the structure generated in (a) around the selected node a “rodlike” structure is generated with the triangular hole pattern on both of its upper faces; (c) using the rodlike structures and a rectangular piece of the stack in (a) a model structure is built for two ridges and the interridge region. In the regions highlighted by lighter circles “stacking faults” help connecting the elements of the model structure.

In the case of the goniometric measurements taking into account that the scales are not laying rigorously in the plane of the wing, but make usually a 10° – 15° angle with this plane, by simple geometric considerations one may conclude that having a 45° incidence with respect to the wing plane and an azimuthal angle of 120° or 240° in backscattering geometry (Fig. 9) is in fact equivalent with a close to normal incidence on the faces of the ridges. Indeed, the twin peaks in Fig. 10(b), are positioned at 480 nm, like the one in normal-incidence specular measurement, and have similar magnitudes in the range of 80%. Under the same conditions, the maximum of the specular reflectance is found at an azimuthal angle of 180° (light incident, emergent in a direction parallel with the ridges) and the spectral position shifted to 422 nm [Fig. 10(a)]. This reflection originates from the structure visible through the windows; the light reflected from the sides of the ridges emerges under different angles.

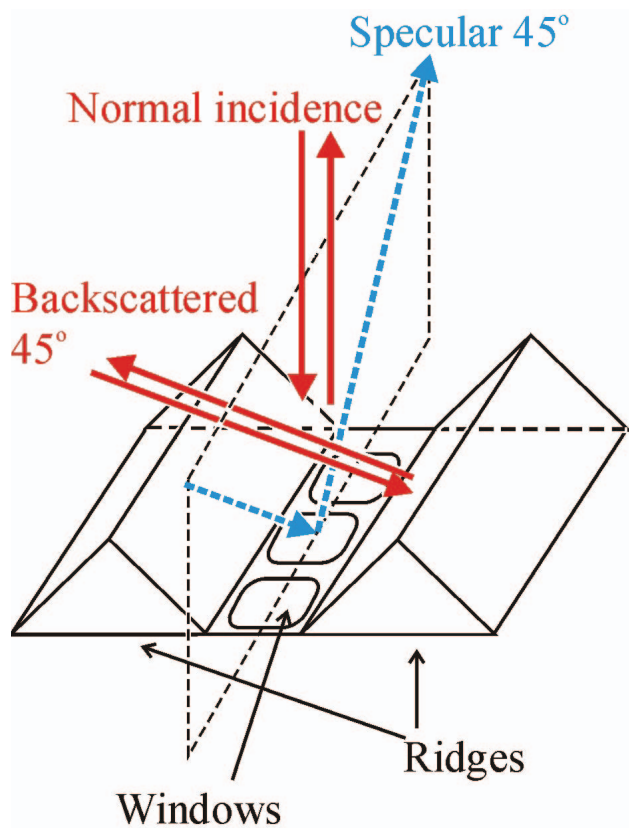


FIG. 15. (Color online) Schematic presentation of the incident and reflected light paths for normal-incidence specular measurement, 45°-incidence specular, and 45°-incidence backscattered geometry.

The peak has a reduced relative intensity in the range of 30%, consistent with the area occupied by the windows.

The reflectance of the inverse opal structure described above can be calculated for normal incidence on different surfaces by using a three-dimensional transfer-matrix technique [24,25]. This computation includes all multiple-scattering effects and is suitable to simulate the specular and diffracted reflectance from a photonic-crystal film as a function of the incident wavelength, the incidence angle, the azimuthal incidence angle, and the incident-wave polarization state. The result of the computation is shown in Fig. 16. The strong blue reflectance found in the calculations arises from the vertical periodicity of the structure. In a simple hexagonal lattice, the vertical stacking distance is just equal to the distance between the holes in the hexagonal basis plane. Here, we have $p=162$ nm. With an average refractive index of 1.4 (arising from a chitin filling factor of 0.75), the dominant reflected wavelength can be estimated to be

$$\lambda = 2p\bar{n} = 454 \text{ nm}. \quad (4)$$

This blue reflection gives rise to the strong band which can be seen in Fig. 16, with a central wavelength just below 450 nm. This very strong reflection can explain the vivid metallic blue of the dorsal face of the wings.

Through a careful analysis of the SEM and TEM data and by the correlation of the information in the two perpendicular

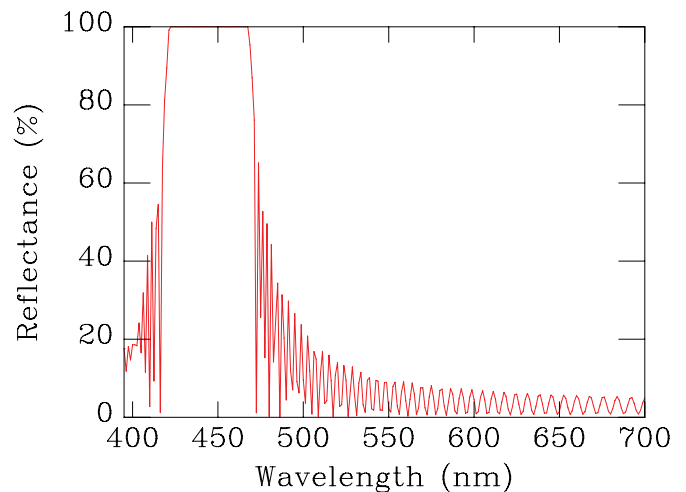


FIG. 16. (Color online) Calculated unpolarized reflectance spectrum for the simple hexagonal stacking of a triangular lattice of holes compatible with the SEM observations.

planes with the reflectance data and computer modeling it was then possible to reveal in a fully consistent way the complete 3D structure of the rather unusual, single-crystalline photonic-crystal-type structure found in the dorsal scales of the butterfly *Cyanophrys remus*.

The ventral sides of the normal and of the bleached butterfly make possible a very interesting comparison: the behavior of the same structure with and without absorbing pigment. Both optical microscopy and spectroscopy revealed that the presence of melanin is a crucial condition for color generation in the structure under investigation. It is remarkable that the ventral scales of the bleached butterfly exhibit the same granular structure as the normal ones (Fig. 4); still, without pigment, they are unable to generate color in the visible, exhibiting a reflectance similar to that of the white diffuse standard [Fig. 8(b)]. As seen in Figs. 4(c) and 4(d), in the regions where some traces of pigments were preserved, a weak blue coloration was present. The reason for the observed blueshift is possibly the decrease of refractive index which follows (on the ground of Kramers-Kronig relations) the decrease of absorption. Some micrographs of the ventral scales revealed some alteration of the surface of certain grains, but many of the grains are practically intact.

From the optical microscopy data, fully confirmed by the SEM micrographs, it is clear that the matt pea-green color arises as a cumulative effect of green, yellow, and blue grains, exposing different facets of fcc inverted opal structure to the incident light. The computed reflectances based on the data extracted from the SEM micrographs (Table II) clearly show that indeed, when white light is incident on different planes of the fcc inverted opal structure, green, yellow, and blue light will be reflected depending on the orientation of the grain. This is clearly confirmed by transfer-matrix simulations which yield the specular reflectance spectra shown in Fig. 17.

In these calculations, the (111) surface is found to very strongly reflect yellow light. This is understandable if one considers the vertical periodicity found in the [111] direction of the fcc structure: the cubic cell diagonal has a length $\sqrt{3}a$,

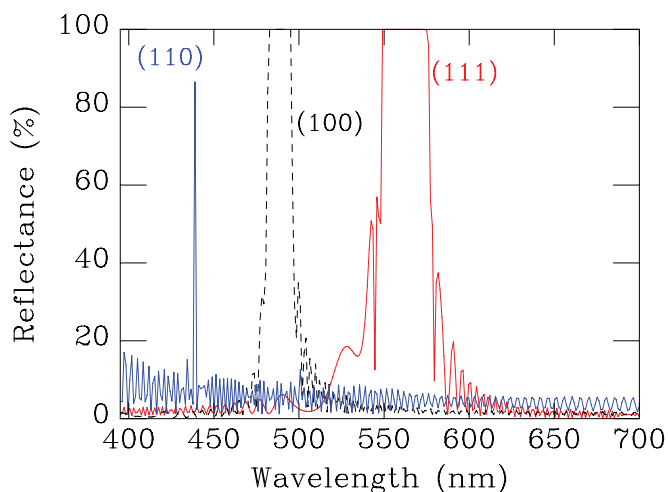


FIG. 17. (Color online) Calculated unpolarized reflectance spectrum for three different surfaces of the inverse opal structure recognized in the grains of the ventral reticulated scales. The incidence is normal on each surface. The (111) surface reflects a rather wide yellow band, and the (100) surface reflects in the bluish-green, while the (110) surface is found to provide a narrow and weaker reflection in the blue.

where $a=395$ nm is the cubic lattice parameter and this length is cut by three reticular planes, equivalent under normal incidence, when the lateral wavelength is virtually infinite. The structure can then be seen, in a first approximation, as a periodic planar multilayer with a vertical periodicity $p = a/\sqrt{3}$. With an average refractive index of $\bar{n}=1.26$, this multilayer is designed to provide a central reflected wavelength of

$$\lambda = 2p\bar{n} = 575 \text{ nm}, \quad (5)$$

which is in the greenish yellow region of the chromaticity diagram. The more detailed calculation of the spectrum shown in Fig. 17 shows the appearance of a reflection band centered at 550 nm.

The (100) surface, also seen in some of the grains, reflects in the bluish green. This, again, can easily be understood in terms of a laterally averaged multilayer structure providing a specular reflection. Here, the periodicity of the (100) reticular planes is $p=a/2$, so that the reflected wavelength is given by

$$\lambda = 2p\bar{n} = 498 \text{ nm}, \quad (6)$$

which will be perceived as a bluish-green coloration. The yellow and bluish green “pixels” are both easily seen in optical microscopy on the ventral scales of the butterfly.

The (110) actually originates from a stop band at the K point, which is the border of the Brillouin zone in the $[110]$ direction. The distance from the origin (Γ point) to this K point is $k=\sqrt{3}(3\pi/2a)$, so that the average-medium dispersion relation predicts the gap opening in the blue at a wavelength

$$\lambda = \frac{2\sqrt{2}}{3}a\bar{n} = 469 \text{ nm}. \quad (7)$$

The spectrum calculation, however, indicates that the reflection is less intense and much narrower than the equivalent bands in the other surfaces.

Goniometric reflectance data [Fig. 10(c)] show that in specular geometry a very weak reflection occurs, most of the light is backscattered [Fig. 10(d)]. This makes it such that the butterfly when resting (Fig. 1) very well blends in the diffuse green background of the vegetation. Together with the observation that the green scales are absent from those regions of the ventral forewing which are covered by the hindwing in resting position [Fig. 2(a)], this is a strong indication that the matt green coloration indeed has a cryptic role.

The way in which the color of the scales on the ventral wing surface is generated may give inspiration for composing” practically any hue of colors from red, green, and blue (RGB color palette) photonic-crystal grains. Interesting practical transpositions may arise, if a structure is found which gives reflection in red, making possible in this way the use of an RGB color palette for artificial photonic crystal displays built of grains similar to those found on the dorsal surface scales of *Cyanophrys remus*. In recent experimental works it was confirmed that it is possible to produce inverted opal-type photonic crystals which appear to be of blue, green, or red color without having to change the structure or the material [26,27]. One of the major technological bottlenecks, however, is connected with the difficulty to produce large-area homogeneous photonic crystals operating in the visible with a precise control of structural perfection. In the biological structure under investigation here, a partial color basis has been defined by conserving the material structure and lattice parameter, and simply changing the orientation of the reflecting surface. A flat panel device containing no radiation source could use such a basis with the orientation being controlled with, for instance, microelectromechanical systems [28]. On the other hand, as demonstrated by our work, for certain practical applications like flat panel displays, smart textiles, electronic papers, etc., it may be more suitable to generate micron size photonic-crystal grains which could be positioned in a given orientation by electric or magnetic fields in order to achieve the colors needed by an RGB palette. As the size of this grains has not to exceed the micron range, their manufacturing may be a lot more simple than obtaining large-size homogenous photonic crystals with band gap in the visible. Such photonic colorants, if based on harmless substances like chitin, may be much more environmentally friendly than many of the pigments based on heavy metals.

To our knowledge the species *Cyanophrys remus* is the only butterfly studied in detail structurally up to now in which two very peculiar photonic-crystal structures were observed: (i) single-crystalline” blue dorsal scales showing long-range order (i.e., on the scale of 100μ); and (ii) granular, polycrystalline photonic crystal of micron size on the ventral, pea-green wing surface composed of individual single-crystalline grains of similar structure like an fcc inverted opal. Although built of somewhat similar elements,

the two kinds of scales accomplish rather opposite functions. The metallic blue dorsal scales may have signaling function while the pea-green ventral scales have cryptic function (Fig. 1). Indeed, the spectral properties of three *Cyanophrys* species sympatric in SE Brazil measured in their dorsal wing surfaces are different in quantitative terms [29]. This observation fully supports the hypothesis that dorsal gleaming coloration has a role in signaling for other individuals. It is worth to point out the versatility and richness of natural designs optimized during evolution. With just one material, chitin, which has a relatively moderate refractive index (1.68), an amazing variety of colors and textures were achieved in one single butterfly. The various photonic structures may accomplish very different functions from signaling to cryptic functions and even thermal management [3].

In a few cases, structures constituted either from single crystal like scales of green color (*Teinopalpus imperialis* Hope, 1843, Papilionidae, Lepidoptera), Argyros *et al.* [22], or from crystalline grains of photonic crystals oriented randomly, also of green color (*Parides sesostris* Cramer, 1779, Papilionidae, Lepidoptera), Vukusic and Sambles [10], were reported. For both butterflies studied in these reports only one side of their wings exhibited photonic crystal structures. Both *T. imperialis* and *P. sesostris* have the photonic-crystal structure on their dorsal side, and their structural color is a vivid green. As opposite to these cases the *Cyanophrys remus* has photonic-crystal structures on both dorsal and ventral sides: a hexagonal primitive lattice (dorsal) and an fcc inverted opal (ventral). Both the metallic blue color (dorsal) and the matt pea-green (ventral) color arise from photonic-crystal-type structures; one is produced by a structure with long-range order, while the other is produced by a random arrangement of blue, green, yellow grains (only local order) of 5–10 μm in size.

IV. CONCLUSION

We investigated the scales of the butterfly *Cyanophrys remus* with experimental methods ranging from optical to electron microscopy and specular, microscopic to goniometric reflectance. Computer modeling was used in various phases of the work to be able to get insight into the structure of the complex objects of study and in the way in which they interact with the probing methods or electromagnetic radiation. The obtained experimental and simulation results show that most frequently one single structural characterization method, like SEM, may give incomplete or erroneous information in the case of such intricately structured objects like photonic crystals in butterfly scales. It is highly recommended that such studies be carried out with various complementary methods.

The electron microscopic investigation (SEM and TEM) of the scale structure combined with FFT analysis has contributed enough information to determine the structure responsible for the color generation in the butterfly scale under study. Although the relative area of the photonic-crystal structure (pepper-pot structure) visible through the windows of the dorsal scales was contradicting the intensity of the blue color, based only on the SEM images it would have

been tempting to exclude the ridges from color generation like is done most frequently when the SEM images of butterfly scales reveal pepper-pot-type structure. As revealed by TEM, in fact, the body of the ridges contains the most important fraction and the most regular part of the photonic-crystal material. Careful structural modeling and reflectances computed on the basis of the structural models allowed us to obtain a fully consistent set of structural and optical data, making possible the accurate identification of the structures responsible for the measured reflectance. The spectrogoniometric measurements proved to be most useful in understanding the role of different structural elements. For reflectors of complex shape both on the micron and submicron scale, like butterfly scales, simple specular or integrated reflectance measurements may prove insufficient.

We showed that the dorsal scales are in fact photonic single crystals of $50 \times 12 \mu\text{m}^2$. To our knowledge hitherto there is no other report published revealing “pepper-pot”-type (a variety of inverted opal) photonic single crystals of this size in butterfly scales.

The dull coloration of the ventral side of the wings is also obtained by structural light filtering. The diffusive mechanism which leads to a dull color, instead of a metallic shine, is related to the use of a photonic polycrystal—an assembly of photonic crystallites of micron size, with a random long-range distribution. The orientation of the crystallites is, by contrast, highly correlated, providing very few types of color pixels, from which the exact optimized hue is obtained.

The investigation of the butterfly *Cyanophrys remus* showed that photonic crystals built of chitin are able to fulfill a wide variety of functions that range from very bright appealing colors to cryptic colors or homogenous neutral coloration when the pigmentation of the photonic-crystal structure has decayed with time. Although built from locally similar elements, the two kinds of scales (single crystalline, metallic blue; polycrystalline, matt green) produce very different visual effects, which is an indication that they could be in relation to different competition benefits. One simple suggestion, supported by measured spectral properties, is that the metallic blue dorsal scales could be involved in signaling functions while the pea-green ventral scales are likely to appear cryptic to some predators.

But the significance of the structure found on the matt side of the wing of *Cyanophrys remus* may be even more far reaching. The association of color pixels from nonpigmentary reflecting microfilters to provide diffusing colored surfaces is an important part of the development of dyes which could avoid heavy-metal pollutants. Smart textiles and papers could assemble micron-size photonic grains or filaments in order to produce optimized visual effects. The physical principles which would allow to describe the appearance of these assemblies do not at the moment show any simple relationship with the principles that explain the structural coloration of the locally ordered individual grains. Much new science can be expected to emerge from the consideration of these unordered assemblies of ordered photonic structures.

ACKNOWLEDGMENTS

The bleached specimen was donated by the Naturhistorisches Museum, Wien (Austria) to Zs. B.; we thank the curators Dr. Sabine Gaal-Haszler and Dr. Martin Lödl for this generosity. We thank Alfred Moser (São Leopoldo, Brazil) for the image we used as Fig. 1. The work was supported by EU6 NEST/PATHFINDER/BioPhot-12915. The work in Hungary was partly supported by OTKA No. 042972. The work in Belgium was partly carried out with support from EU5 Centre of Excellence ICAI-CT-2000-70029 and from

the Inter-University Attraction Pole (IUAP P5/1) on “Quantum-size effects in nanostructured materials” of the Belgian Office for Scientific, Technical, and Cultural Affairs. L.P.B, K.K., and Z.V. wish to thank the Hungarian Academy of Sciences and the Belgian FNRS for financial support. V.L. was supported as by the Belgian National Fund for Scientific Research (FNRS) and Stanford University (USA). This work has been partly supported by the European Regional Development Fund (ERDF) and the Walloon Regional Government under the “PREMIO” INTERREG IIIa project.

-
- [1] K. Ohtaka, Phys. Rev. B **19**, 5057 (1979).
 [2] E. Yablonovitch, Phys. Rev. Lett. **58**, 2059 (1987).
 [3] L. P. Biró *et al.*, Phys. Rev. E **67**, 021907 (2003).
 [4] J. D. Joannopoulos, R. D. Meade, and J. N. Winn, *Molding the Flow of Light* (Princeton University Press, Princeton, 1995).
 [5] A. Chutinan, S. John, and O. Toader, Phys. Rev. Lett. **90**, 123901 (2003).
 [6] M. Imada, A. Chutinan, S. Noda, and M. Mochizuki, Phys. Rev. B **65**, 195306 (2002).
 [7] K. Srinivasan, P. E. Barclay, O. Painter, J. Chen, A. Y. Cho, and C. Gmachl, Appl. Phys. Lett. **83**, 1915 (2003).
 [8] E. J. Reed, M. Soljacic, and J. D. Joannopoulos, Phys. Rev. Lett. **90**, 203904 (2003).
 [9] A. R. Parker, Mater. Today **5**, 26 (2002).
 [10] P. Vukusic and J. R. Sambles, Nature (London) **424**, 852 (2003).
 [11] G. Tayeb, B. Gralak, and S. Enoch, Opt. Photonics News **2**, 40 (2003).
 [12] S. Kinoshita, S. Yoshioka, Y. Fujii, and N. Okamoto, Forma **17**, 103 (2002).
 [13] A. Parker, J. R. Soc., Interface **2**, 1 (2005).
 [14] M. Doebeli and U. Dieckmann, Nature (London) **421**, 259 (2003).
 [15] Z. Bálint, Z. Vértésy, and L. P. Biró, J. Nat. Hist. **39**, 2935 (2005).
 [16] S. Berthier, *Iridescences, les couleurs physiques des insectes* (Springer-Verlag, Paris, 2003).
 [17] S. Berthier, E. Charron, and J. Boulenguez, Insect Sci. **13**, 145 (2006).
 [18] R. K. Robbins and M. Duarte, Proc. Entomol. Soc. Wash. **107**, 398 (2005).
 [19] R. K. Robbins, J. Lepid. Soc. **34**, 194 (1980).
 [20] H. Ou-Yang, G. Stamatias, and N. Kollias, J. Invest. Dermatol. **122**, 492 (2004).
 [21] R. J. D. Tilley and J. N. Eliot, Trans. Lepid. Soc. Jpn. **53**, 153 (2002).
 [22] A. Argyros, S. Manos, M. C. J. Large, D. R. McKenzie, G. C. Cox, and D. M. Dwarde, Micron **33**, 483 (2002).
 [23] P. Vukusic, J. Sambles, C. Lawrence, and R. Wootton, Proc. Biol. Sci. R. Soc. London **266**, 1403 (1999).
 [24] J. B. Pendry and A. MacKinnon, Phys. Rev. Lett. **69**, 2772 (1992).
 [25] J. Vigneron and V. Lousse, Proc. SPIE **6128**, 61281G (2006).
 [26] A. A. Zakhidov, R. H. Baughman, Z. Iqbal, C. Cui, I. Khayrullin, S. O. Dantas, J. Marti, and V. G. Ralchenko, Science **282**, 897 (1998).
 [27] Z.-Z. Gu, H. Uetsuka, K. Takahashi, R. Nakajima, H. Onishi, A. Fujishima, and O. Sato, Angew. Chem., Int. Ed. **42**, 894 (2003).
 [28] A. E. Franke, T.-J. King, and R. T. Howe, MRS Bull. **26**, 291 (2001).
 [29] K. Kertész, Zs. Bálint, Z. Vértésy, G. I. Márk, V. Lousse, J. -P. Vigneron, and L. P. Biro Curr. Appl. Phys. **6**, 252 (2006).